Design of a 1 DOF MEMS motion stage for a parallel plane geometry rheometer

Yong-Sik Kim, Nicholas G. Dagalakis, Chiara Ferraris, and Svetlana Avramov-Zamurovic

Abstract— Rotational rheometers are used to measure paste properties, but the test would take too long to be useful for quality control (QC) on the job site. In this paper, a new type of rheometer is proposed based on a one degree of freedom (DOF) micro-electro-mechanical systems (MEMS)-based motion stage. Preliminary data will be presented to show the capability of the system to measure the viscoelastic properties of a paste. The parallel plate geometry rheometer consists of two plates, which move relative to each other to apply a strain to the material to be tested. From the stress measured and the strain applied, the rheological characteristics of the material can be calculated. The new device consists of an electrothermal actuator and a motion plate. For the rheological measurements, the device is designed to generate the shear stress up to 60 Pa and maintain its stiffness to less than 44 N/m. With these features, the device uses a square plate of 1.5 mm x 1.5 mm to provide enough area for a few micro-liter level volumes. The motion of the square plate is monitored by a capacitive sensor at the end of the oscillating plate which has a resolution of 1.06 μm. When a reference cementitious paste, Standard Reference Material (SRM)-2492, is placed between the oscillating plate of the presented motion stage and a fixed plate, the reduction in the displacement of the oscillating plate is monitored showing that the presented motion stage is reasonably designed to detect the response of the reference cementitious paste.

Index Terms— MEMS, motion stage, electrothermal actuator, rheology, cement paste.

Y.-S. K. Author is with Intelligent Systems Division, Engineering Laboratory, National Institute of Standards and Technology, 100 Bureau Dr. Gaithersburg, MD, 20899, USA; e-mail: mk37do@gmail.com).

N. G. D. Author is with Intelligent Systems Division, Engineering Laboratory, National Institute of Standards and Technology, 100 Bureau Dr. Gaithersburg, MD, 20899, USA.

C. F. Author is with Materials and Structural Systems Division, Engineering Laboratory, National Institute of Standards and Technology, 100 Bureau Dr. Gaithersburg, MD, 20899, USA.

S. A. Z. is with Weapons and System Department United States Naval Academy, 105 Maryland Avenue, Annapolis, MD 21402, USA.

I. INTRODUCTION

RHEOLOGICAL measurements of viscoelastic materials, especially cement pastes, are critical to obtain desirable material properties in civil engineering and related applications [1]. Concrete is the main material used in infrastructure construction (bridges, buildings...) and is composed of cement, water, sand, aggregate, and chemical additives. The rheological properties of concrete are related to the relative amounts of the components used especially to the rheological properties of the cement paste. The cement paste is composed of cement, water, and chemical additives. Cement could also be a blend of Portland cement and other fine powders such as fly ash and limestones. Thus a fast measurement method of the rheological properties of the cement paste would allow the engineer to optimize the concrete composition [2].

Rotational rheometer designs used to measure properties of cementitious materials from concrete [3, 4] to cement paste include parallel plates or concentric cylinders [5]. The principle of a rotational rheometer is to shear the material between two surfaces, by rotating one surface at a controlled speed and measuring the resulting torque. If the gap between the shearing surfaces is small enough, there are analytical equations to calculate the viscosity of the material. The rotation surface could rotate at a constant speed or oscillate at various frequencies [6, 7]. In this paper, the oscillatory method will be used.

To test cementitious materials, the commonly used oscillatory frequency ranges are between 0.2 Hz [6] and 1 Hz [7] depending on its application. The gaps between two plates are reported to be around 0.4 mm to 0.65 mm [2, 6]. In cement pastes, the general grain size is about 80 μm to 100 μm [5]. The measured shear or storage modulus varies from 100 Pa to 1.3 MPa [7]. Based on these data a micro electro mechanical systems (MEMS) rheometer for cement pastes was designed.

The idea to use MEMS technologies in rheological measurements for cement paste was motivated by the goal of building a cheap, disposable rheometer that could be used for quality control (QC) in the field. Conventional rotational rheometers like Thermo Scientific HAAKE MARS Rheometer[1] are expensive and are not portable. Moreover, it

would be advantageous to run multiple measurements at the same time of various composition of the paste to explore the influence of additives dosage or type on the cement paste rheological properties. Thus, a rheometer based on micro-electro-mechanical systems [8] would be advantageous. MEMS devices are small and low-cost [9, pp. 50–51], and can be designed to be mounted to run multiple experiments at the same time [10]. For the MEMS-based rheometer, the parallel plate geometry rheometers were used due to their simple structure.

A MEMS-based linear motion stage replaces the oscillating plate in the parallel plate rotational rheometers, and uses an optical method to measure their motion [8]. The electrostatic actuators are commonly used in MEMS-based linear motion stages for their long range motions but need a clean environment for their operations [11]–[13]. The rheometer has to apply enough shear force and be stable against materials that would flow outside the shearing plates, so thermal actuators are desirable for rheological systems for their milli-Newton level force and reliable operation under dirty or harsh environment.

This paper describes design and fabrication of 1 degree of freedom (DOF) linear motion stage for rheological measurement. This stage is composed of an actuator, an oscillating plate, and eight folded springs and each component is analyzed in the following section. An electrothermal actuator is adapted as an actuator and designed for its reliable operation in dusty environments [14], [15]. A capacitive displacement sensor is attached at the end of the oscillating plate to monitor its behavior and the large square plate of micro-scale level is used to hold the paste tested. This device is fabricated based on Silicon-on-Insulator Multi-User Multi-Processes (SOI-MUMPs) [16] and tested with a cementitious reference material, SRM-2492 [17] composed of an aqueous solution of corn syrup and limestone powder. The experimental results are obtained with the MEMS based 1 DOF linear motion stage and its application in a parallel plate rotational rheometer is discussed..

II. DESIGN OF THE MEMS-BASED 1 DOF MOTION STAGE

Figure 1 illustrates the conceptual model of the parallel plate type MEMS-rheometer. The rheometer is composed of two plates; a stationary plate and an oscillating plate. A material will be placed between the two plates. In this paper, the stationary plate is an ordinary glass substrate and the oscillating plate will be replaced by the MEMS-based 1-DOF motion stage. When the oscillating plate applies a shear force to a material, its corresponding displacement is measured by the embedded sensor. The oscillating plate is a 1.5 mm x 1.5 mm square plate and is able to contain up to a few micro-liters of cementitious materials. The displacement and the shear force can be used to calculate the rheological properties of the material.
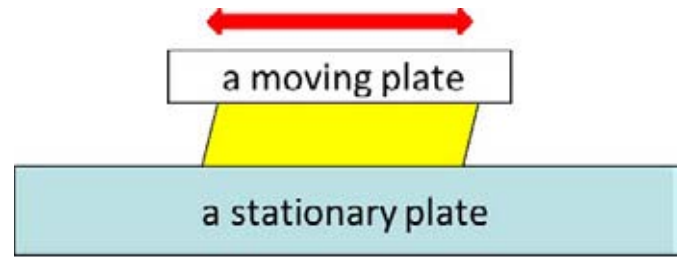
Fig. 1. The parallel plates type rheometer

The 1-DOF motion stage is composed of one dual-bent beam electrothermal actuator, an oscillating plate, and one embedded capacitive sensor and its schematic diagram is shown in Fig. 2(a). The oscillating plate is supported by eight folded springs which hold the plate in position and minimize its out-of-plane deformation when a test material is placed between the two plates. The dual bent-beam type electrothermal actuator consists of two bent-beam type electrothermal actuators in a series. With a serial connection, this actuator reduces its stiffness to 50 % of single bent-beam type electrothermal actuator, which makes the motion stage respond with more sensitivity during a material test. The details for each component are described in the following sections.

A. The analysis for the dual-bent beam electrothermal actuator

The schematic model of the presented motion stage is illustrated in Fig. 2(a). In the dual bent-beam electrothermal actuator, two bent-beam type electrothermal actuators are connected to the same lateral bar. This serial connection reduces its stiffness in half, but the analytic relationship for the bent-beam actuator is still valid. There is a similar actuator reported as a one-ring spring actuator [18], where this lateral bar is thermally isolated and operates as a mechanical constraint. In this paper, the lateral bar is used to simply connect two bent-beam type actuators, because perfect thermal insulation of the lateral bar is hard to implement with MEMS fabrication technologies.

In this case, the total stiffness of the actuator, K_{act} can be expressed as a serial connection of two bent-beam actuators as

$$\frac{1}{K_{act}} = \frac{1}{K_{bent}} + \frac{1}{K_{bent}} \quad \text{or} \quad K_{act} = \frac{K_{bent}}{2} \qquad (1)$$

where K_{bent} is the stiffness of the bent-beam type actuator. The output displacement of the motion platform will be expressed based on a parallel connection of springs as:

$$U_{plat} = \frac{F_{act}}{K_{act} + K_{plat}} \qquad (2)$$

where F_{act} is the force generated by the dual bent-beam type actuator, and K_{plat} is the stiffness of the oscillating plate. Each term is explained in the following section.
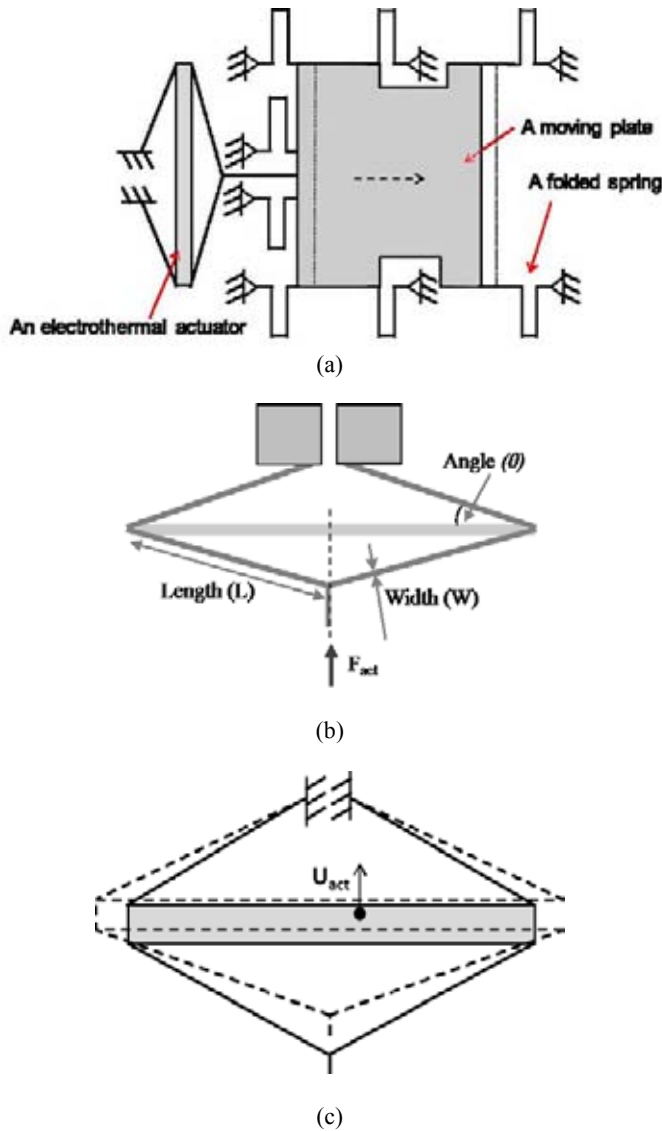
Fig. 2. The schematic model; (a) the presented 1-DOF motion stage; (b) the dual bent-beam electrothermal actuator; (c) the expected mechanical behavior of (b)

The schematic design of the presented dual bent-beam electrothermal actuator is shown in Fig. 2(b). The dual bent-beam is based on the thermal expansion of the lateral beam when the current flows through the actuators, whose expected behavior is shown in Fig. 2(c). In Fig. 2(c), the solid line stands for its original shape and a dotted line represents the expanded shape. Based on this mechanism, the stiffness of the actuator can be expressed [19] as:

$$K_{act} = n\frac{\sin^2\theta EWT}{L} \qquad (3)$$

where n is beam number, E is Young's modulus of silicon, W is the beam width, L is the beam length as described in Fig. 2(b), and T is the beam thickness. Equation (3) expects the stiffness of the presented dual bent-beam actuator would be 43.04 N/m based on the design parameters listed in Table 1.

As expected, this value is a half of the original bent-beam type actuator. The stiffness calculated in finite element analysis (FEA) is 43.7 N/m. These values indicate equation (3) predicts the stiffness with the error of less than 1 %.

The expected force from the actuator, F_{act} can be expressed based on a beam theory [20] and the geometric relationship between the lateral bar and two bent-type actuators as:

$$F_{act} = \alpha\Delta T_{ave}ET(W_{lateral}\tan\theta - 2nW\sin\theta) \qquad (4)$$

where α is coefficient of thermal expansion of silicon, ΔT_{ave} is an average temperature rise of the actuator, $W_{lateral}$ is the beam width of the lateral beam and T is the thickness, and Θ is the beam angle of the bent-beam actuator. Based on these relationships, the main design parameters are set and listed in Table 1.

TABLE I
THE DESIGN PARAMETERS IN THE PRESENTED MOTION STAGE

Symbol	Design parameter	Values
W	Actuator beam width	22.37 µm
θ	Actuator beam angle	0.8 degrees
L	Actuator beam length	2350 µm
T	Actuator beam thickness	30 µm
n	Number of beams in actuator	5
L_{spring}	Folded spring link length	1000 µm
L_s	Folded spring short link length	100 µm
W_{spring}	Folded spring link width	15 µm
W_s	Folded spring neck length	100 µm
K_{plat}	The stiffness of the oscillating plate	51.76 N/m
K_{act}	The stiffness of the actuator	43.7 N/m

B. The folded springs

The folded spring shown in Fig. 3 supports the four corners of the oscillating plate, and is a compliant mechanism which transmits a translational motion without significant loss or motion error. The folded spring is made up of three cantilever beams and is located at corners and near the actuator as shown in Fig. 2(a). The main purpose of the eight springs is not only to allow only one directional motion, but also to reduce any out-of-plane deformation of the oscillating plate.
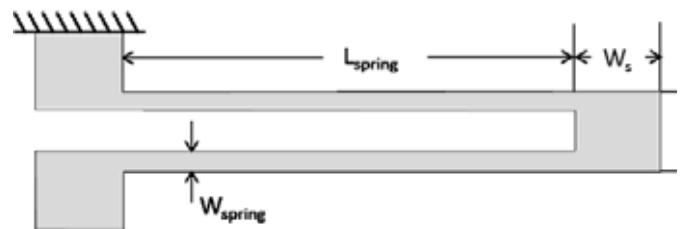

Fig. 3. The design of the folded spring

The stiffness of the oscillating plate is the summation of the stiffness of the eight folded springs [18] and can be expressed as:

$$\frac{2}{K_{plat}} = \frac{1}{ET}\left(\frac{L_{spring}^3}{2W_{spring}^3} + \frac{6(1+\mu)L_{spring}}{5W_{spring}} + \frac{L_s}{2W_s} + \frac{3L_{spring}^3 Ls}{2W_s^3}\right) \quad (5)$$

where μ is the Poisson's ratio of silicon, and the other design parameters are indicated in Fig. 3. The value for each design parameter is listed in Table 1. Based on these geometries, the stiffness of the oscillating plate is about 53.4 N/m based on equation (3). With the design parameters described above, equation (2) can be extended as:

$$U_{plat} = \frac{2\alpha EWT\sin\theta}{3kp\left(n\sin^2\theta\frac{EWT}{L} + K_{plat}\right)}V^2 \quad (6)$$

where α is the coefficient of thermal expansion of silicon, K_{plat} is given by Eq. (5), and V is the driving voltage applied to the actuator. Equation (6) indicates that the displacement of the motion stage is proportional to the square of the driving voltage.

III. FINITE ELEMENT ANALYSIS (FEA)

Finite element analysis (FEA) simulation [21] is also utilized to verify the analysis described above and predict the thermal and structural behavior of the presented motion stage. The material properties used in the FEA are cited from a previous publication [20] and the same wafers are utilized in the fabrication. In this simulation, the ends of the eight folded springs and the ends of the actuator are assumed to be firmly fixed for structural analysis and they are connected to a heat sink at room temperature of 20 ℃ for thermal analysis.

The expected mechanical behavior is calculated in FEA and plotted in Fig. 4(a). This is the response corresponding to the excitation by the driving voltage of 5 V. This is calculated to result in the temperature rise of 542.6 ℃. This temperature value is close to the maximum endurable limit of silicon; 550 ˚C [22], so the displacement by this can be interpreted as the maximum displacement of the motion stage without any permanent damage. The stress distribution is also visualized based on von Mises stress in Fig. 4(b). The expected maximum stress will be 193 MPa and distributed near the folded springs. Most deformation occurs near the folded springs and the actuator when the oscillating plate is in its operation. This indicates that the stiffness of the folded spring and the square plate are well adjusted. In addition to this, the maximum value is far less than the yield strength of silicon 7 GPa, so the calculated displacement shown in Fig. 4(a) is expected to be repeatable without any permanent damage.
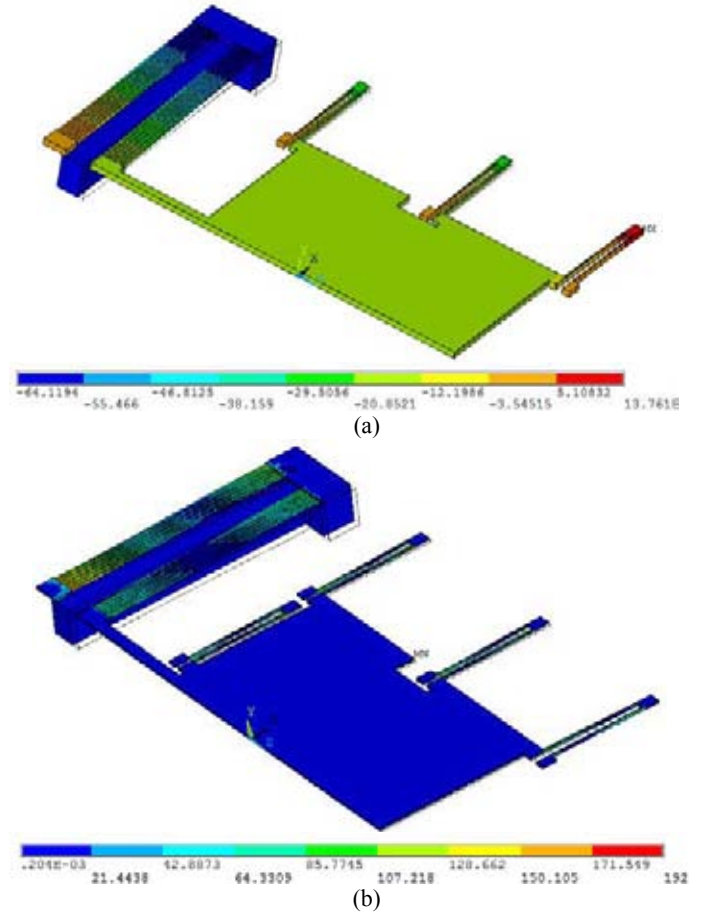
(a)

(b)

Fig. 4. FEA simulation results by the temperature rise up to 542.6 ℃; (a) the displacement vector sum (in μm unit); (b) von Mises stress distribution over the stage (in MPa unit)
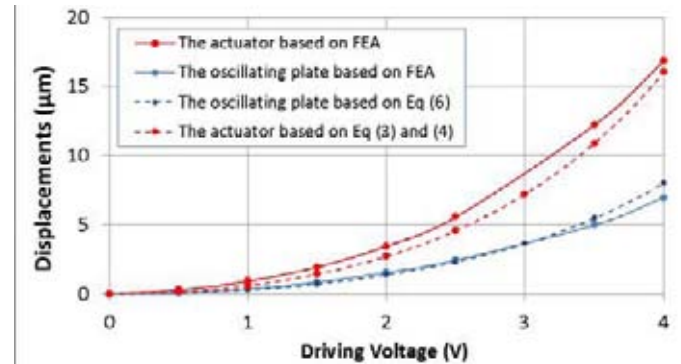
Fig. 5. The calculated displacement of the oscillating plate and the actuator from FEA and analytic relationship

The relationship between the driving voltage and the corresponding output displacement is also inspected in FEA. The displacement of the oscillating plate is calculated based on the driving voltage and plotted in Fig. 5. The actuator is expected to generate more motions than the oscillating plate. This behavior is also compared with the analytic relationship from the previous section; the displacement of the motion stage is calculated based on Eq (6) and that of the actuator is from Eq (3) and Eq (4). These calculations are plotted in

dotted lines in Fig. 5, which indicates that the analytic relationship in the previous section shows reasonable trends

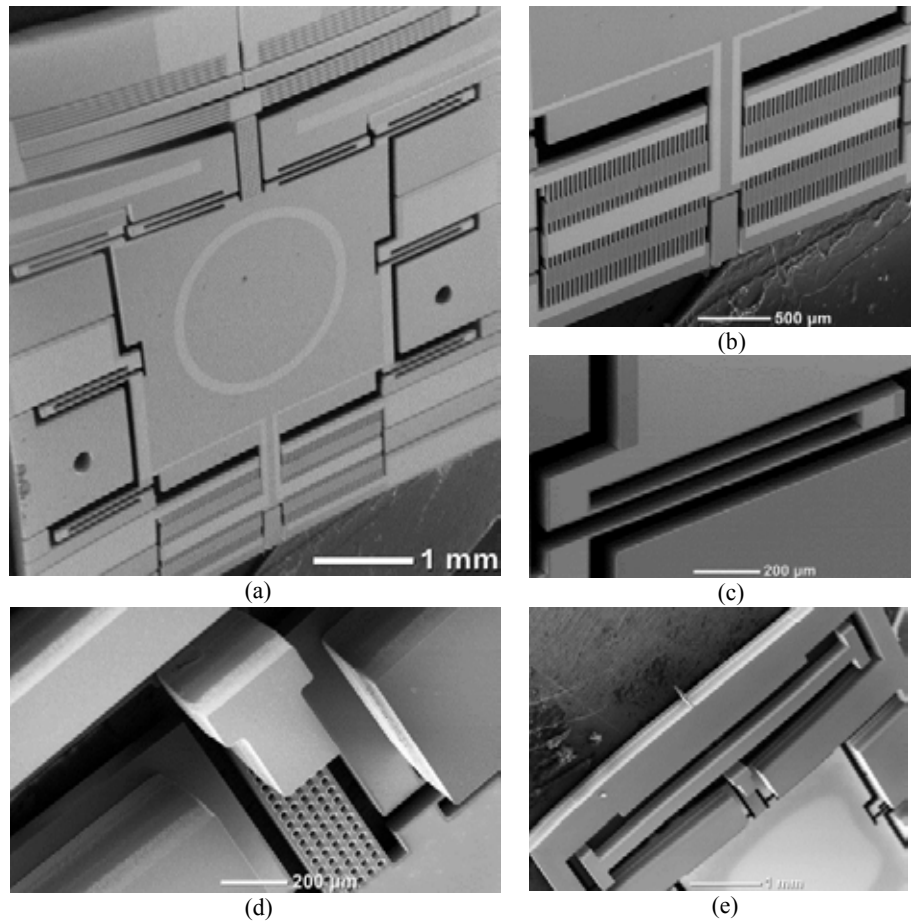compared with FEA, as a function of the driving voltage.

Figure 6: SEM images of a fabricated motion stage; (a) a frontal full view, (b) an embedded capacitive sensor, (c) a close-up view of a the folded spring, (d) the connecting block underneath the lateral bar in (e), (e) the backside view of the lateral bar in the actuator

IV. MICRO-FABRICATION

The fabrication process for the oscillating plate follows standard MEMS fabrication processes: Silicon-On-Insulator Multi-User Multi-Processes (SOI-MUMPs) [16] and a Silicon-On-Insulator (SOI) wafer. The SOI wafer used for the presented motion stage consists of a 30 μm thick device layer, a 400 μm thick handle layer, and a 2 μm thick buried oxide layer. The fabrication process consists of four steps – one metal deposition process on the device layer of a SOI wafer, two deep reactive ion etching (DRIE) processes for the device layer and the handle layer of an SOI wafer, and the removal process of a buried oxide layer. The details about this fabrication are described in details in a similar MEMS-based motion stage study [20].

Based on the fabrication procedure described above, the presented motion stage has been fabricated with an embedded capacitive sensor. Their detailed images are shown in Fig. 6, where the bright white areas are electric paths for the actuator and the embedded capacitive sensors. Grey areas are made of silicon and black areas are holes through the wafer. The full frontal view of the presented motion stage is shown in Fig.

6(a), where the dual bent-beam electrothermal actuator, the oscillating plate, and the embedded capacitive sensor are linked to each other. Figure 6(b) is the detailed image of the embedded sensor, which is made up of multiple interdigitated fingers and able to generate differential output from two pairs of finger groups to eliminate resident capacitance. The close-up view of the folded spring is shown in Fig. 6(c), where the bright line is an electric wire conductive path for the embedded capacitive sensor. The actuator is electrically disconnected from the oscillating plate by a physical gap, which is supported by the connecting block underneath it in Fig. 6(d). Figure 6(e) is the backside of the actuator. The lateral bar underneath the actuator will hold the whole actuator for reliable operation.

V. EXPERIMENTAL RESULTS

The mechanical response of the presented motion stage and the embedded capacitive sensor was experimentally evaluated. For this experiment, two metal pads near the actuator are electrically connected to direct current (DC) power supply units (Agilent Model 3322A[1]) to control the actuator. The two

electrodes and one ground of the embedded capacitive sensor are connected to an Analog Device[1] single channel Capacitive-to-Digital converter AD7747[1] [22], which converts the capacitance change into voltage information for computers. With these features, the displacements of the oscillating stage are measured separately by an optical profiler (VEECO[1] NT1100 [23]), which will be used as a reference value to evaluate the capabilities of the embedded capacitive sensor.
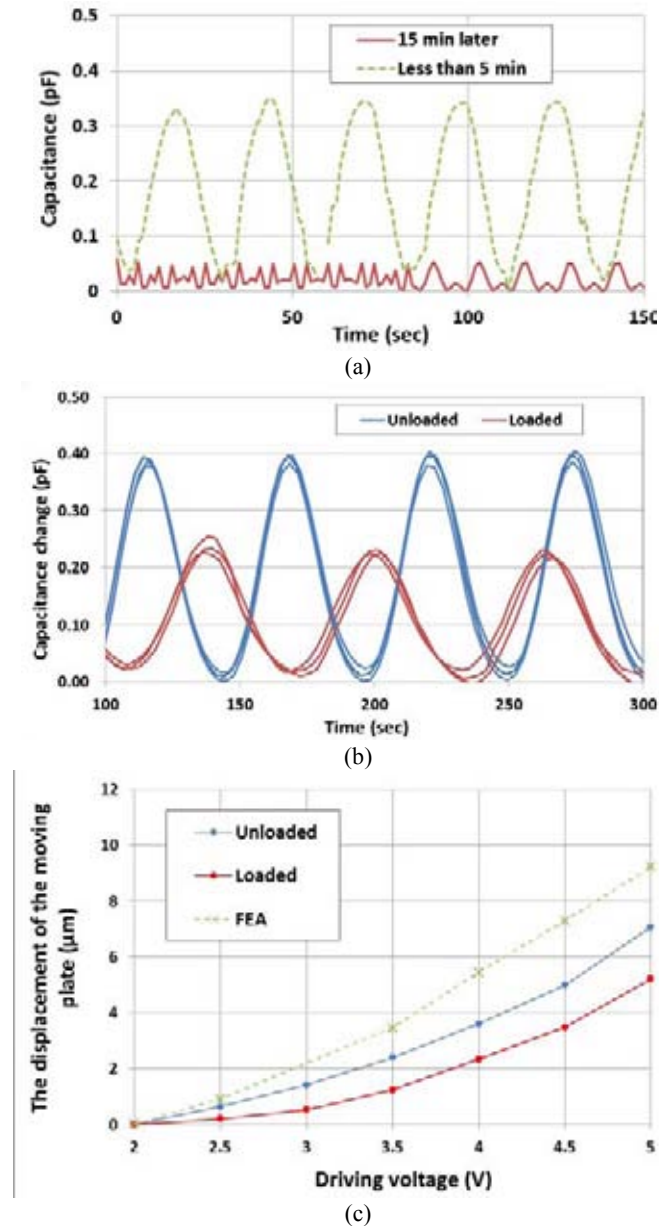

(a)

(b)

(c)

Figure 7: Experimental results of the displacement of the motion stage for two cases; sample loaded and unloaded: (a) the motion after the paste is exposed to air, (b) the difference of the capacitance with a paste being loaded and unloaded, (c) the capacitance change of (b) as a function of a driving voltage

The embedded sensor measured the capacitance change from the motion from a few microns to tens of microns. Based on the measurements from NT1100[1], the capacitance-to-displacement ratio of the embedded sensor was obtained, which is 106.41 µm/pF. The Capacitive-to-Digital converter chip has the accuracy of 10 fF, so the resolution of the

embedded sensor is expected to be 1.06 µm. With this calibrated sensor, the displacement of the oscillating plate is measured through the embedded capacitive sensor, when the cementitious material is loaded and unloaded, respectively. The operating frequency used for all the tests was 0.5 Hz and various displacements are tested. The corresponding experimental results are shown in Fig. 7.

Water will evaporate from the paste material when exposed to the atmosphere and thus the particles will interlock, as shown in Fig. 7(a). With the reference material SRM-2492, the results obtained less than 5 min after being placed on the oscillating plate have no significant change, but the values are really low after 15 min, indicating a significant change in the material, probably due to water evaporation. Based on this observation, all tests are done within 5 min after the sample is exposed to air.

Figure 7(b) shows the reduction of the displacements of the oscillating plate when a sample material is loaded between the oscillating plate and a fixed plate as described in Fig. 1. The reference material for the paste rheometers is placed on the stationary plate with a nano-liter syringe [24]. After the reference material is placed between the two plates, the size of the physical gap between the two plates will be measured with the NT1100 and the approximate contact area of the material is visually measured under a microscope. The motion of the oscillating plate decreases by about 44 % when the target material is loaded. This reduction indicates that the design of the presented motion stage is designed reasonably to be sensitive to the changes due to a sample and the embedded sensor is able to detect the change of the motion to this degree. This difference is plotted and compared with FEA as a function of a driving voltage in Fig. 7(c). The cases with a sample loaded and unloaded show a similar pattern with the expectation based on FEA.

The shear rate and displacement of the oscillating plate will be controlled by the amplitude of the injection voltage and its operating frequency. Figure 8 shows the various motions with the driving voltage from 2 V to 5 V showing that the different shear rate is expected with the presented motion stage. Based on these experimental data and the analytic relationship, a Bingham model [25] can be built for further analysis later. These are preliminary data but it shows that MEMS could be used to measure the rheological properties of paste. Further tests are needed and also, a wider range of shear rate would be desirable to probe ranges that are useful in the construction industry.
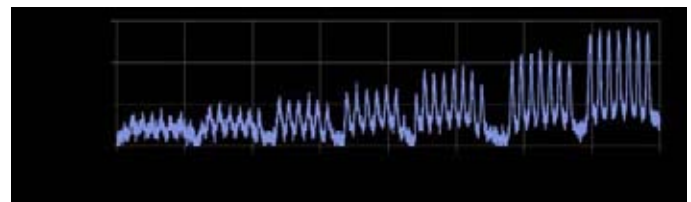

Figure 8: Capacitance sensor output for different actuator driving voltage amplitude rates

VI. CONCLUSION

The design, fabrication, and testing of a MEMS based motion stage has been presented for rheological properties measurement of paste type materials. This MEMS based system is designed to replace the parallel plate rotational rheometers. For the rheological application, the presented motion stage adopts (1) the dual bent-beam type electrothermal actuator for a low stiffness operation, (2) a large square plate to contain enough cementitious material, (3) an embedded capacitive sensor to monitor the displacement of the motion stage, and (4) derive a Bingham mathematical model to represent cementitious materials. Through these procedures, the presented rheometer is able to generate rheological data of up to the shear rate of 0.0275 1/s and the shear stress of 45 Pa.

Compared with conventional rheometers, this MEMS-based rheometer provides more detailed information in a relatively short shear rate range. Design optimization or a new design concept is needed to compensate the missing shear rate change. Further analysis and tests are required to apply for new applications such as biomedical or gels for their viscoelastic properties.

REFERENCES

[1] Brower, Lynn and Ferraris, Chiara F., "Comparison of Concrete Rheometers: International Tests," *Concr. Int.*, pp. 41 – 47, Vol. 25 #8,2003

[2] C. F. Ferraris, Measurement of the rheological properties of cement paste: a New Approach, Int. RILEM Conf., *The role of Admixtures in High Performance Concrete*, J. G. Cabrera and R. Rivera-Villareal, eds., Monterrey (Mexico) March (1999) pp. 333-342 (http://ciks.cbt.nist.gov/monograph/)..

[3] C. Ferraris, L. Brower editors, "Comparison of concrete rheometers: International tests at LCPC (Nantes, France) in October 2000", *NISTIR 6819*, 2001 (http://fire.nist.gov/bfrlpubs/build01/PDF/b01074.pdf)

[4] C. Ferraris, L. Brower editors, "Comparison of concrete rheometers: International tests at MB (Cleveland OH, USA) in May 2003", *NISTIR 7154*, 2004 (http://ciks.cbt.nist.gov/~ferraris/PDF/DraftRheo2003V11.4.pdf).

[5] G. Marin, A. A. Collyer, and D. W. Clegg, *Rheological Measurements*. Collyer, AA, Clegg, D. W., Eds, 1988.

[6] L. J. Struble and M. A. Schultz, "Using creep and recovery to study flow behavior of fresh cement paste," *Cem. Concr. Res.*, vol. 23, no. 6, pp. 1369–1379, 1993.

[7] Z. Sun, T. Voigt, and S. P. Shah, "Rheometric and ultrasonic investigations of viscoelastic properties of fresh Portland cement pastes," *Cem. Concr. Res.*, vol. 36, no. 2, pp. 278–287, 2006.

[8] G. F. Christopher, J. M. Yoo, N. Dagalakis, S. D. Hudson, and K. B. Migler, "Development of a MEMS based dynamic rheometer," *Lab. Chip*, vol. 10, no. 20, pp. 2749–2757, 2010.

[9] M. J. Madou, "*Fundamentals of microfabrication*. 2002," Boca Raton Fla. CRC Press, vol. 200, pp. 298–205.

[10] K. A. Ronaldson, A. D. Fitt, A. R. H. Goodwin, and W. A. Wakeham, "Transversely Oscillating MEMS Viscometer: The 'Spider,'" *Int. J. Thermophys.*, vol. 27, no. 6, pp. 1677–1695, 2006.

[11] Q. Yao, J. Dong, and P. M. Ferreira, "Design, analysis, fabrication and testing of a parallel-kinematic micropositioning XY stage," *Int. J. Mach. Tools Manuf.*, vol. 47, no. 6, pp. 946–961, 2007.

[12] D. Mukhopadhyay, J. Dong, E. Pengwang, and P. Ferreira, "A SOI-MEMS-based 3-DOF planar parallel-kinematics nanopositioning stage," *Sens. Actuators Phys.*, vol. 147, no. 1, pp. 340–351, 2008.

[13] Y. Ando, "Development of three-dimensional electrostatic stages for scanning probe microscope," *Sens. Actuators Phys.*, vol. 114, no. 2, pp. 285–291, 2004.

[14] J.-S. Park, L. L. Chu, E. Siwapornsathain, A. D. Oliver, and Y. B. Gianchandani, "Long throw and rotary output electro-thermal actuators based on bent-beam suspensions," in *Micro Electro Mechanical Systems*, 2000. MEMS 2000. The Thirteenth Annual International Conference on, 2000, pp. 680–685.

[15] W.-C. Chen, P.-I. Yeh, C.-F. Hu, and W. Fang, "Design and characterization of single-layer step-bridge structure for out-of-plane thermal actuator," *Microelectromechanical Syst. J. Of*, vol. 17, no. 1, pp. 70–77, 2008.

[16] K. Miller, A. Cowen, G. Hames, and B. Hardy, "*SOIMUMPs design handbook*," MEMSCAP Inc Durh., 2004.

[17] Ferraris C.F., Stutzman P., Winpigler J., Guthrie W., "Certification of SRM 2492: Bingham Paste Mixture for Rheological Measurements" , *SP-260-174 Rev. 2012*, June 2012 (http://www.nist.gov/manuscript-publication-search.cfm?pub_id=911268)

[18] J. K. Luo, A. J. Flewitt, S. M. Spearing, N. A. Fleck, and W. I. Milne, "Three types of planar structure microspring electro-thermal actuators with insulating beam constraints," *J. Micromechanics Microengineering*, vol. 15, no. 8, p. 1527, 2005.

[19] J. K. Luo, A. J. Flewitt, S. M. Spearing, N. A. Fleck, and W. I. Milne, "Modelling and fabrication of microspring thermal actuator," in *Nanotech 2004 Vol.1: Technical Proceedings of the 2004 NSTI Nanotechnology Conference and Trade Show*, vol. 1, Nano Science and Technology Institute, 2004, pp. 355–358.

[20] Y.-S. Kim, J.-M. Yoo, S. H. Yang, Y. M. Choi, N. G. Dagalaks, and S. K. Gupta, "Design, fabrication and testing of a serial kinematic MEMS XY stage for multifinger manipulation," *J. Micromechanics Microengineering*, vol. 22, no. 8, 2012.

[21] ANSYS Fluent, "*12.0 User's Guide*," User Inputs Porous Media, p. 6, 2009 on http://www.ansys.com.

[22] Analog Device, AD7747, 24-bit, 1 channel capacitance to digital converter on http://www.analogdevice.com.

[23] "Dynamic MEMS Measurement Option for Wyko NT1100 Optical Profilers." on http://www.veeco.com

[24] "MICROMAN." Positive-displacement pipet, M10 model on http://www.gilson.com/Pipette/Products/44.224

[25] Hackley V. A, Ferraris C.F., "The Use of Nomenclature in Dispersion Science and Technology" NIST Recommended Practice Guide, SP 960-3, 2001, http://fire.nist.gov/bfrlpubs/build01/art108.html